Bahar Davoudi*, Dana Gasumova, Kostadinka Bizheva, Robert Dinniwell, Wilfred Levin and I. Alex Vitkin

Quantitative assessment of oral microstructural and microvascular changes in late oral radiation toxicity, using noninvasive *in-vivo* optical coherence tomography

Quantitative Bewertung oraler mikrostruktureller und mikrovaskulärer Veränderungen bei Patienten mit später oraler Radiotoxizität mittels der nicht-invasiven optischen Kohärenztomographie *in-vivo*

DOI 10.1515/plm-2015-0025
Received July 24, 2015; revised November 4, 2015; accepted November 9, 2015

Abstract

Background and objectives: About half of the head and neck cancer patients treated with radiotherapy suffer from late radiation effects months to years after the treatment. The most common diagnosis and monitoring methods for such oral toxicities are based on surface examination of the oral tissue, which is subjective. Therefore, subsurface imaging and image quantification tools can be highly useful for monitoring these late effects as these approaches are more robust and objective. In this study, we demonstrate the ability of optical coherence tomography (OCT) technology and its newly developed quantitative imaging platform to reveal subsurface microstructural and microvascular changes in late oral radiation toxicity patients, not detectable by available clinical tools.

Materials and methods: Fifteen patients exhibiting late oral radiation toxicity, and five healthy age-matched volunteers were imaged with OCT in a clinical pilot study. Image assessment methods, developed in-house, were used to extract four quantitative metrics of potential clinical importance from the acquired microstructural and microvascular oral OCT images.

Results: The statistically significant differences in the patients compared to healthy volunteers were: lower epithelium to lamina propria thickness (indicating epithelial atrophy and/or fibrosis of lamina propria), smaller vessel diameter (indicating vessel lumen narrowing), and higher blood velocity. The observed *in-vivo* morphological changes correlated well with reported histology findings. No significant changes were observed in vessel tortuosity between the cohorts.

Conclusion: The quantitative metrics extracted from the OCT images demonstrated significant microstructural and microvascular differences between the two cohorts. Potentially, OCT and its newly developed image analysis platform can be used as a noninvasive *in-vivo* subsurface tool for "shedding light" on late oral radiation toxicity, for example in palliative treatment efficacy monitoring.

Keywords: late radiation side effects; normal tissue response to radiation; optical coherence tomography (OCT); Doppler OCT; speckle variance OCT; quantitative analysis; high resolution imaging.

***Corresponding author: Bahar Davoudi,** Medical Biophysics Department, University of Toronto, MaRS/TMDT building, 101 College Street, 15th floor, Toronto, ON M5G 1L7, Canada, e-mail: bahar.davoudi@utoronto.ca
Dana Gasumova and I. Alex Vitkin: Medical Biophysics Department, University of Toronto, MaRS/TMDT building, 101 College Street, 15th floor, Toronto, ON M5G 1L7, Canada
Kostadinka Bizheva: Department of Physics and Astronomy, University of Waterloo, 200 University Avenue West, Waterloo, ON N2L 3G1, Canada
Robert Dinniwell and Wilfred Levin: Princess Margaret Cancer Center, 610 University Avenue, Toronto, ON M5G 2M9, Canada

Zusammenfassung

Hintergrund und Zielsetzung: Etwa die Hälfte der Patienten mit Krebserkrankungen im Hals-Kopf-Bereich, die sich einer Strahlentherapie unterzogen haben, leiden noch Monate bis Jahre nach der Behandlung an Strahlenspätschäden. Die häufigsten Diagnose- und Monitoringmethoden zur Feststellung von oralen Toxizitäten basieren dabei

auf der Untersuchung der Gewebeoberfläche und sind deshalb subjektiv. Unter die Oberfläche „blickende“ Bildgebungsverfahren in Kombination mit entsprechenden Quantifizierungstools können daher für die Überwachung dieser Spätschäden sehr nützlich sein, da sie robuster und objektiver sind. Die vorliegende Studie zeigt, dass es möglich ist, mittels der optischen Kohärenztomographie (OCT) und einer neu entwickelten quantitativen Imaging-Plattform unter der Oberfläche liegende mikrostrukturelle und mikrovaskuläre Veränderungen bei Patienten mit später oraler Toxizität zu identifizieren, die mit verfügbaren klinischen Instrumenten nicht nachweisbar sind.

Material und Methoden: Im Rahmen einer klinischen Pilotstudie wurden 15 Patienten mit oraler Spättoxizität und 5 gesunde Probanden gleichen Alters mittels OCT untersucht. Ein eigens entwickeltes Bildbewertungsverfahren wurde genutzt, um vier quantitative Kenngrößen von potenzieller klinischer Bedeutung aus den gewonnenen mikrostrukturellen und mikrovaskulären OCT-Bildern zu extrahieren.

Ergebnisse: Es ergaben sich folgende statistisch signifikanten Unterschiede bei den Patienten im Vergleich zu den gesunden Probanden: geringere Epithel/Lamina Propria-Dicke (als Hinweis auf eine Epithelatrophie und/oder Fibrose in der Lamina propria), kleinere Gefäßdurchmesser (als Anzeichen für eine Gefäßverengung) und höhere Blutgeschwindigkeit. Die *in vivo* beobachteten morphologischen Veränderungen korrelieren gut mit histologischen Beschreibungen. Hingegen wurden keine signifikanten Veränderungen der Gefäßtortuosität zwischen den Kohorten beobachtet.

Fazit: Die aus den OCT-Bildern extrahierten quantitativen Kenngrößen zeigten signifikante mikrostrukturelle und mikrovaskuläre Unterschiede zwischen den beiden Kohorten. Potenziell könnte das beschriebene OCT-Verfahren zusammen mit der neu entwickelten Bildanalyse-Plattform als nicht-invasives *In-vivo*-Werkzeug genutzt werden, um orale Strahlenspätschäden zu diagnostizieren, zum Beispiel in der Palliativmedizin zur effektiven Patientenüberwachung.

Schlüsselwörter: Strahlenspätschäden; normale Gewebereaktion auf Bestrahlung; Optische Kohärenztomographie (OCT); Doppler OCT; Speckle-Varianz-OCT; quantitative Analyse; hochauflösende Bildgebung.

1 Introduction

The majority of the head and neck cancer patients undergo radiation therapy at some point during their curative treatment [1–3]. Even though treatment methods such as intensity modulated radiation therapy have resulted in better dose conformity and contributed to more accurate tumor targeting [4], nearly all treated patients develop radiation toxicity in their healthy oral tissue [3]. This includes early radiation effects (e.g. mucositis) which typically repair within a few weeks after radiotherapy [5, 6], or late complications (e.g. xerostomia, soft tissue ulceration, fibrosis, and osteoradionecrosis) which are often more complex and debilitating [6]. These take longer to heal and are usually associated with scarring and loss of function [6]. Late complications are reported in about half of the head and neck cancer patients who undergo radiotherapy [1]. They often lead to impaired oral intake, problems with swallowing and speech, and other quality of life detriments [3, 7].

Currently, the diagnosis and evaluation of these conditions is based on visual inspection and palpation of the oral tissues, and clinical assessments using common toxicity scoring scales, e.g. the Radiation Therapy Oncology Group (RTOG) scoring [1], and symptom-based questionnaires filled out by the patients [1]. Nonetheless, it has been well established that late oral radiation toxicity does not begin on the tissue surface but in the subsurface tissue compartments due to stromal, parenchymal, and vascular damage, which then produces the typical clinical surface appearances [8, 9]. Fibrosis is the major stromal change that arises from radiation damage to the vasculature and augmented vessel permeability [6, 10, 11], leading to fibrin deposition, collagen formation, and reduction of parenchymal function [6, 11, 12]. Parenchymal damages manifest when the rate of destruction of epithelial cells exceeds the rate of replacement with competent fully functional cells [3, 8]. Vascular damage typically involves vessel lumen narrowing due to myointimal proliferation in arterioles and venules [8, 10]. Also, thrombus formation causes lumen narrowing which can lead to capillary obstruction [8, 10, 12]. Damage of endothelial cells in venules and capillaries has been suggested as a source of cytokines which stimulate epithelial cell proliferation, resulting in elongated and tortuous vessels (i.e., telangiectasia) that try to compensate for the totally or partially occluded vessels [10].

The available knowledge on the mechanisms of late radiation effects has been mostly derived from *ex-vivo* histology-based research studies [8]; however, histology (tissue biopsy) is rarely used in current clinical practice, as it delays healing, may increase the size of the lesion, increases the risk of infection and can lead to tissue break down. Besides, although histology is useful for confirming the cause of suspicious lesions, it does not give any functional information, such as characteristics of the

blood supply and circulation, which can be important. Therefore, a noninvasive technique that can provide high resolution, volumetric sub-surface images of the morphology and vasculature in the oral tissue may be of high value for clinical assessment of late oral radiation toxicity. Moreover, utilizing an image quantification platform to analyze the tissue images can strengthen the assessment of such complications and help in gaining a better understanding of their origins and mechanisms of progression.

Several imaging methods have been used for clinical assessment of the structural or vascular alterations in oral tissue with oral radiation toxicity. These techniques include texture analysis and size measurement of salivary or parotid glands in ultrasound [13–15], magnetic resonance imaging (MRI) [16, 17] and computed tomography images [18]. In an attempt to assess vascular involvement, dynamic contrast-enhanced MRI has been used to investigate perfusion characteristics of late radiation toxicity of these glands [17, 19]. Even though these studies have succeeded in highlighting changes using some image quantification, they limited their investigations to the salivary and parotid glands. Also, due to suboptimal spatial resolution, the focus of these studies was on macroscopic features based on an ensemble of subsurface layers or microvascular networks, rather than directly resolving the structure of interest, monitoring the tissues layer by layer, or investigating single microvessels.

Optical coherence tomography (OCT) is a noninvasive *in-vivo* imaging modality that provides fine detail of the microstructure and microvasculature of biological tissue, owing to its micron-scale resolution [20]. This optical imaging technique, based on the difference in light scattering and absorption properties of various tissue compartments, visualizes tissue to a depth of ~1–2 mm beneath the tissue surface [20]. Owing to these features, OCT has started to attract attention in oral mucosal imaging through the use of fiber optic probes and catheters to monitor a variety of oral malignancies [21–26] as well as mucositis, an acute radiation therapy side effect [21, 23, 25, 26]. In monitoring early radiation toxicity with OCT, most of the studies have been conducted on animals and very few have imaged human subjects [21, 26]. These studies mainly concentrated on assessing structural OCT images, and only one (in an animal model) also evaluated microvascular alterations due to early radiation toxicity [25]. To date, no studies have been reported using OCT to monitor late radiation complications (neither structural nor vascular). Therefore, to quantitatively address this unmet clinical need, we used a research-grade OCT system in a clinical pilot study to image microstructural and microvascular alterations in the oral tissues of patients with late oral radiation toxicity. An image assessment platform was also developed to extract microstructural and microvascular metrics (such as layer thickness, blood velocity, vessel diameter, and vessel tortuosity) from the acquired OCT images. These metrics were then compared between patients and healthy volunteers to evaluate whether there were significant differences between the two cohorts. To our knowledge, this is the first time OCT has been used to assess and quantify late oral radiation toxicity in human subjects.

2 Materials and methods

2.1 Clinical study

The cross-sectional feasibility study [27] was approved by the Research Ethics Board of Princess Margaret Cancer Center (Toronto, Canada) and was carried out on 15 patients (mean age, 56.7±12 years) and five healthy volunteers (mean age, 58.2±8 years). None of the healthy volunteers had any known comorbidities. Relevant patient information is summarized in Table 1. The imaging session for each subject (including preparation, acquiring images and data acquisition) took about 20–45 min, during which ~6–20 volumetric microstructural and microvascular OCT image data sets were acquired and stored for later analysis and quantification. For the patients, images were typically taken from various oral regions (mostly from the labial tissue and/or the soft palate if it was accessible). Several three-dimensional (3D) OCT images were captured from each site by slightly moving the oral probe around (4–10 mm in accessible directions). Whenever the clinician identified a symptomatic region, images were also captured from that site and its mirror site on the contralateral side.

2.2 OCT system and images

An OCT imager and a specialized oral probe were designed and built to operate at the central wavelength of 1310 nm, offering an axial resolution of 5.1 μm in biological tissue [28]. The lateral resolution of the OCT system was ~20 μm. The total optical power incident on tissue surface was approximately 6 mW, which is well below the ANSI recommended maximum permissible exposure for that spectral region [29]. Cross-sectional OCT images were collected at the rate of 47,000 lines/s, which minimized motion artefacts in the OCT tomograms. A typical 3D OCT image

Table 1: Relevant patient information.

Patient number	Age (years)	Gender	Years since radiation therapy	Tumor location	Clinical problem[a]
1	47	M	4	Tonsil	ORN
2	58	M	9	Left buccal, alveolus and base of tongue	Trismus, xerostomia, fibrosis
3	55	F	2	Tongue	Neck fibrosis, mucosal changes in cheeks and tongue
4	69	M	9	Nasopharynx	Bilateral sensorineural hearing loss
5	73	M	2	Left base of tongue	Xerostomia, dysphagia, pain in neck and jaw
6	70	F	7	Sinus	Neck fibrosis, lymphedema
7	69	M	8	Maxillary sinus	ORN
8	61	M	2	Right base of tongue	Neck fibrosis, xerostomia, dysphagia
9	62	F	9	Right tongue	ORN
10	53	M	8	Hard palate, right retromolar trigon	ORN, soft tissue necrosis
11	52	F	7	Right tongue	ORN, trismus
12	58	M	9	Right tongue	Fibrosis of right neck
13	65	M	1	Left retromolar trigon	ORN
14	41	M	4	Nasopharynx	Right hypoglossal weakness
15	28	M	6	Nasopharynx	Neck fibrosis

M, Male; F, female; ORN, osteoradionecrosis.

[a]At the first visit to the Adult Radiation Late Effects Clinic at the Princess Margaret Hospital, Toronto.

represented a tissue volume of 1 mm×1 mm×~1 mm corresponding to 200 pixels×200 pixels×512 pixels, the first two dimensions representing the lateral field-of-view and the third representing the depth. The imaging setup was designed so that the patient sat on a chair in front of the rigid oral probe (17 cm long and 2 cm in diameter), with the chin and forehead on a chin-rest and forehead-rest, respectively (similar to an eye examination setup) [28]. The probe was inserted into the oral cavity of the patient to obtain images without touching the tissue.

To validate our methodology, we previously acquired microstructural OCT images of pig oral tissue *ex-vivo* and compared them to histology of the same regions demonstrating excellent agreement [28]. OCT images were also acquired of healthy volunteers *in-vivo*, and close similarity of these images to published OCT images of the same oral regions was confirmed [30]. The epithelium (Ep) manifested as the low scattering top most layer. Lamina propria (LP) appeared as a bright highly scattering layer with blood vessels running through it. In the soft palate, the elastin layer showed as bright dispersed patches in a dark background. In certain tissue types (such as labial), the submucosa was also discernible as a low scattering region in which glands could be found as dark circular or oval regions with highly scattering walls [28]. These comparative studies were highly beneficial since in the current pilot clinical study, we were not permitted to obtain histological samples from any of the participants, due to the invasive nature of biopsy and the risks associated with it (augmented discomfort, infection development, and ulcer or fistula formation in the oral cavity).

2.3 Quantification of microstructural and microvascular features

OCT images acquired during the clinical study were comprised of microstructural and microvascular categories. The microstructural images provided grayscale depth reflectivity profiles representing the Ep, LP, and in many cases the submucosa. The microvascular visualization included both Doppler and speckle variance OCT (svOCT) images. The former provided information on blood flow in the vessels non-perpendicular to the interrogating beam direction [31, 32], and the latter offered 3D visualization of microvessels (diameter >10 μm), but no blood flow information [33–36]. From these, we extracted a number of microstructural and microvascular metrics, based on a number of expected biological outcomes of late oral radiation toxicity [34, 37]. A list of these metrics, the type of information they represent, and the biological rationale behind each is provided in Table 2. The first metric (Ep/LP thickness) was calculated through a costume-developed MATLAB code that asked the user to delineate the Ep and LP, and then performed the calculation of the thickness ratio of these two layers based on the input [37]. For each 3D data set, this procedure was repeated for 15 different A-scans chosen from different B-scans and the average was calculated as the final Ep/LP thickness for

Table 2: List of calculated metrics based on OCT images (microstructural and microvascular).

#	Metric	Oral site	Source image	Indication
1	Ep/LP thickness	Soft palate	Structural OCT	Epithelial atrophy and/or fibrosis of LP
2	Vessel diameter	Labial	svOCT	Change in vessel lumen size
3	Vessel tortuosity	Labial	svOCT	Whether vessels have become "twisty and bendy"
4	Blood velocity	Labial, soft palate	Doppler OCT	Alteration in blood flow characteristics

Ep, Epithelium; LP, lamina propria; OCT, optical coherence tomography; svOCT, speckle variance OCT.

that particular data set. The second and third metrics (vessel diameter and tortuosity) were measured manually over the segmented vessels in the svOCT images (in ImageJ program) [34]. The fourth metric (blood velocity) was calculated using a developed MATLAB code which required the user to delineate the vessel boundaries [34]. The detailed methodology for calculating these metrics has been explained previously [34, 37].

Tissue vascular tree in the oral tissue encompasses capillaries, arterioles, venules, and small arteries and veins. Radiation likely alters all these components. However, based on the phase noise level and spatial resolution characteristics of our OCT system, we were not able to monitor the capillaries (diameter <10 μm). Therefore, vascular quantification was based on the measurement of vessels of ~15–100 μm in diameter (including arterioles, venules, small arteries and small veins) [8]. In the vascular quantifications, "vessel" was defined as any segment of the vascular network in the svOCT image that was considered a separate branch. It has been shown that some capillaries become occluded as a result of radiation damage, causing others to enlarge as a compensation mechanism [9]. Such telangiectasic capillaries may have also been included in our analysis since they fell in the diameter range we monitored.

2.4 Statistical analysis

The significance of the observed differences in the four developed metrics between the patients and healthy volunteers was calculated using a Mann-Whitney rank-sum test [38]. The non-normal distribution of the acquired data necessitated the use of such a ranking-based significance test. To perform it, the patient group involved all the images from various oral sections in the patients which received >50 Gy (maximum dose to the tumor) [39], and the healthy volunteer group consisted of all the images from various oral sections in the volunteers.

The statistical significance level of the difference between the two cohorts was found using the *t*-test table for very large number of samples ($n \to \infty$) [38]. It has been shown that for a large number of samples, the variables of a non-parametric test (i.e., z values) can be transformed to those of a parametric test (i.e., *t* values) [38]. In such cases, the *p*-values corresponding to the $n = \infty$ column of a *t*-table are used to find the significance levels [38].

3 Results

Different oral regions (labial and soft palate) in the patients and healthy volunteers were imaged using the OCT system and the oral probe. Most of the late radiation effects have been reported to occur after a cumulative dose of 50 Gy [8]. Therefore, we only included the patient images which were taken from the oral regions that received >50 Gy (based on the radiation dose plan) as late radiation toxicity lesions. In this section, the OCT images from the same oral region of the two cohorts are first compared qualitatively. Afterwards, the results of quantitative comparison of the four developed metrics (Table 2) between the patients and healthy volunteers are presented.

3.1 OCT images: qualitative analysis

Figure 1A and B show structural OCT images of the soft palate in a healthy volunteer and a patient, respectively. Ep thinning (top dark layer) and thickened LP (bright, highly scattering layer), suggesting fibrosis, are noticeable in the patient's soft palate. While the elastin layer is represented as white short stripes beneath the LP in Figure 1A, this layer is not discernible in Figure 1B. The increased scattering of the LP leading to decreased light penetration can be the main reason for elastin invisibility. Figure 1C demonstrates a normal labial tissue comprising of LP, filled with vessels, covered by the Ep. Figure 1D corresponds to the labial tissue of a severe fibrosis case. This patient was treated before the intensity-modulated radiation therapy era and had to undergo full dental extraction due to major osteoradionecrosis of the jaw and tooth decay as the sequalae. The layer differentiation between the Ep

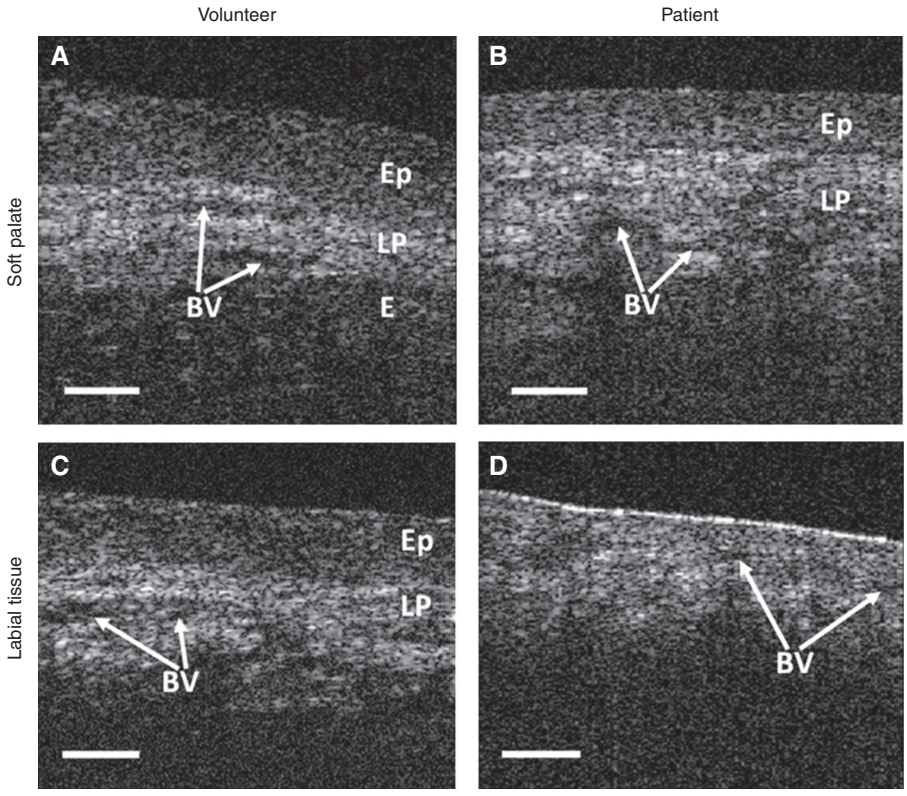

Figure 1: Grayscale microstructural OCT images. (A) A healthy volunteer's compared to (B) a patient's soft palate showing epithelium (Ep) thinning, thickened lamina propria (LP) and loss of elastin (E) in the patient. (C) The labial tissue of a healthy volunteer. (D) The labial tissue of a severe late radiation toxicity case. Total layer disruption is noticeable in (D). No changes in blood vessels (BV) can be concluded from these images. Features are best visible in supplementary three-dimensional multimedia files (supplementary materials 1–4). Darker colors represent high absorption regions (such as Ep) and brighter colors show higher light scattering (such as LP). Scale bars: 200 μm.

and LP is completely lost. Imaging depth has decreased due to a high amount of scattering as a result of severe fibrosis.

In Figure 2, typical Doppler OCT images of a healthy volunteer (Figure 2A and C) and a patient (Figure 2B and D) are shown. Doppler OCT monitors the velocity of erythrocytes along the interrogating beam (in this case, depth) direction. Therefore, the vessels running horizontally (at 90° to the incident OCT beam) are not detected. Comparing Figure 2A and C with Figure 2B and D, there is a ~2× increase in the patient's blood velocity compared to the healthy volunteer. Despite this observed difference, such qualitative analyses based on single images are not robust enough to be used as clinical tools.

The acquired svOCT images were combined to reconstruct a 3D map of the microvasculature [34]. Figure 3 shows such a 3D map for a healthy volunteer (Figure 3A and B) and a patient (Figure 3C and D). No comparison can be made on the difference in vessel anatomical features (such as average diameter) between the two cohorts, without proper quantitative analysis.

3.2 Quantitative analysis

The quantitative assessment platform was developed to extract one metric from the microstructural and three from the microvascular (Doppler and svOCT) images. The results from comparing these metrics between the two cohorts as well as the *p*-values calculated through the Mann-Whitney rank-sum test are shown in Figure 4. Figure 4A shows a comparison of the first metric (Ep/LP thickness, Table 2) in about 40 regions within the soft palate of seven patients (which received >50 Gy) and in about 50 regions in five healthy volunteers. This metric could not be calculated on some patients due to the following reasons: (1) in three cases, severe radiation-induced damage caused loss of distinction between the Ep and LP, making their thickness measurement impossible (and in fact showing more pronounced radiation damage); (2) in three other cases, the imaging probe could not access the soft palate due to presence of neck fibrosis or trismus leading to immobility of the head and inability to open the mouth more than 2 cm, respectively; (3) in the two remaining cases,

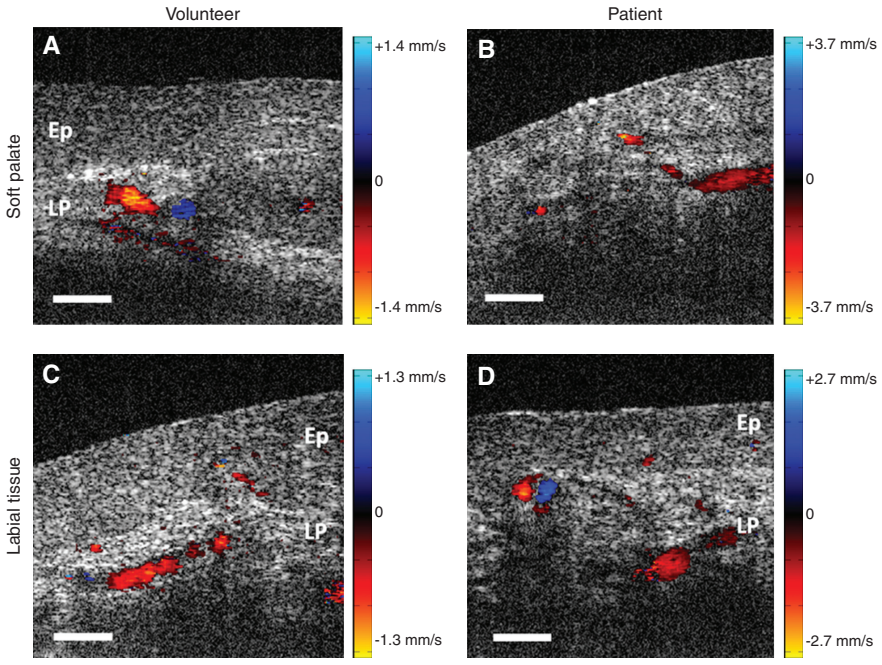

Figure 2: Doppler images of blood vessels overlaid on structural OCT images. Soft palate in a healthy volunteer (A) compared to a patient (B), and labial tissue of a healthy volunteer (C) compared to a patient (D). Generally, higher blood velocity is detected in the patients' vessels (B and D) compared to the healthy volunteers (A and C). The velocity values demonstrated here correspond to the axial flow component of erythrocytes. Blue and red hues correspond to two different flow directions. Ep, epithelium; LP, lamina propria. Scale bars: 200 μm.

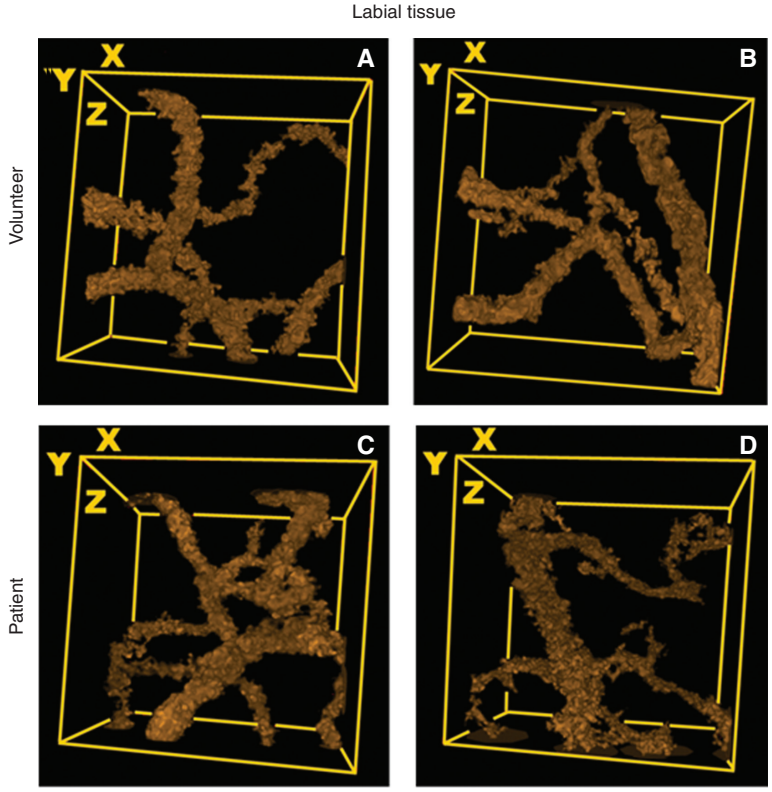

Figure 3: Three-dimensional speckle variance OCT images of the vasculature map in the labial tissue. (A) and (B) healthy volunteers, (C) and (D) late oral radiation toxicity patients. No conclusion can be drawn on the size and abundance of vessels by visual inspection of these images, and more thorough calculations must be performed to derive meaningful quantitative metrics. Field-of-view is 1 mm×1 mm×0.5 mm (xyz), where z is along the depth dimension.

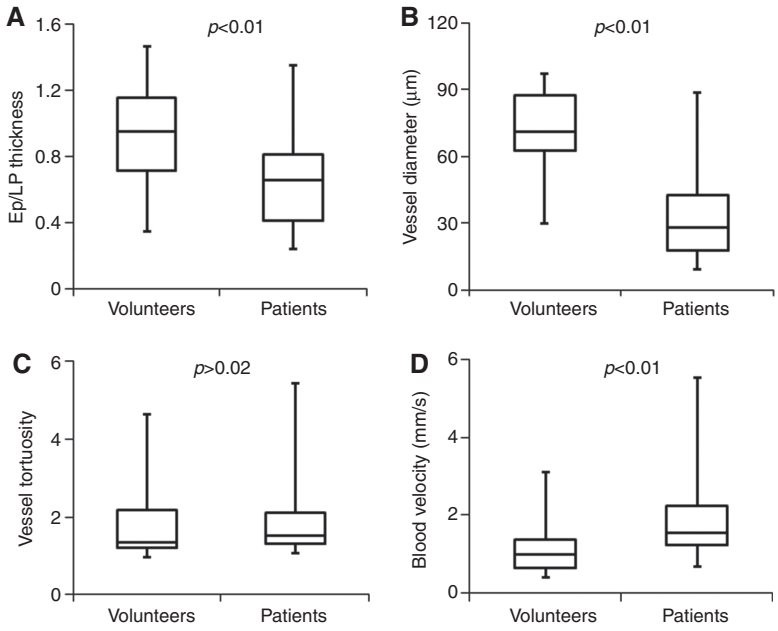

Figure 4: Box-and-whisker plots of the four developed OCT image quantification metrics. (A) Epithelium to lamina propria (Ep/LP) thickness, (B) blood vessel diameter, (C) vessel tortuosity, and (D) blood velocity. (A) is calculated from structural OCT images, (B) and (C) from speckle variance OCT and (D) from Doppler. The *p*-values, obtained from Mann-Whitney rank-sum significance test demonstrates a highly significant difference for (A), (B), and (D) between the two cohorts, and no significant difference in (C). In a box and whisker plot, the top error bar shows the range of the largest 25% of the data (when data is sorted in an ascending order), the top box demonstrates the second largest 25%, the lower box the third 25%, and the lower error bar shows the smallest 25%. The border between the two boxes marks the median of the data.

one had involuntary tremors and the other was not able to sit for the session and requested early termination of imaging. Figure 4A suggests a significantly lower Ep/LP thickness in the patient cohort, corresponding to Ep thinning, increased LP thickness (which may be attributed to fibrosis), or both ($p<0.01$). This metric could only be calculated for the cases in which the Ep and the LP were still discernible. Due to severity of the radiation damage, there were several cases with complete loss of layer definition, such as the one shown in Figure 1D.

Moving on to microvascular quantification (second metric), Figure 4B demonstrates a comparison between the measured diameters in about 40 vessels (with diameter <100 μm) in four patients and 50 in four healthy volunteers, based on svOCT images. The svOCT images of the fifth volunteer suffered from high degree of tissue motion and thus were not suitable for the quantification analysis. The low number of patient images eligible for this metric calculation was due to the fact that svOCT is prone to motion artifact and therefore it could only be acquired from regions that were easier to stabilize (such as labial tissue) rather than regions such as soft palate that were more affected by involuntary motions such as breathing. Furthermore, for most of the patients, the labial tissue was out of major radiation field (and thus received lower than 50 Gy). So while the labial tissue was the most stable site for svOCT imaging, it typically did not satisfy the criteria for being a late toxicity site (dose >50 Gy), leading to a lower number of eligible patients for svOCT-based metrics. However, the total number of vessels from these few patients that were included in the svOCT-related metrics was relatively high (more than 100) and adequate for statistical analysis. In the results, a significant vessel lumen narrowing was observed in the patient group ($p<0.01$). The next metric based on svOCT microvascular images was the microvessel tortuosity (third metric). In Figure 4C, this parameter is compared between 65 microvessels in the same four patients and 90 in four healthy volunteers. No significant difference was observed between the tortuosity in the two cohorts ($p>0.02$). Figure 4D shows the difference in the blood velocity (fourth metric) between about 80 microvessels (of diameter <100 μm) in 12 patients and about 60 in five healthy volunteers. This graph suggests a significantly higher blood velocity in the patient group ($p<0.01$).

4 Discussion

OCT is a noninvasive, non-hazardous, subsurface imaging modality, with possible application for the assessment of

stromal and vascular changes that might be associated with late radiation effects where obtaining a biopsy poses additional risks and discomfort for the patients. The OCT imaging and image quantification platform developed in this study enabled objective assessment of the observed microstructural and microvascular changes in oral tissues of patients with late oral radiation toxicity. To evaluate the clinical value of the platform, the results of this quantitative assessment will be compared to the expected histological and biological changes in late oral radiation toxicity cases as documented in pathology reference texts.

A common complication associated with late oral radiation toxicity is epithelial thinning [3, 8]. This happens when the Ep involutes at a higher rate than it regenerates [3, 8]. By developing and measuring the Ep/LP thickness metric, our aim was to demonstrate this change quantitatively. The analysis did show a significantly lower value in the patients which can be attributed to a thinner Ep (due to mucosal atrophy) or thickened LP (because of accumulated collagen causing fibrosis) [12], or both.

Fajardo et al. [8] have discussed that vessel lumen obstruction frequently occurs as a manifestation of late damage to the arterioles, venules, small arteries and small veins. This happens mainly due to fibrosis of the adventitia or the intima, although mild fibrosis of the media can also occur. Thrombus formation can also lead to vessel blockage [6, 8]. In the current study, we measured the diameter of medium-sized vessels from the acquired svOCT images and confirmed that the average vessel diameter in late oral radiation toxicity patients was significantly lower than in the healthy volunteers. Another possible vascular damage is the development of more tortuous vessels, especially venules and capillaries [8]. Vascular damage may lead to more tissue injury through ischemia, which stimulates endothelial cell proliferation with consequent deformity of the capillaries which become tortuous and elongated [40]. Others have proposed that weakening of the vessel wall can result in twists and bends in the vessel [8]. In the current study, a metric was developed to calculate vessel tortuosity in medium-sized vessels and was compared between the two cohorts [34]. The analysis, however, did not show a significant difference between vessel tortuosity in the patients and healthy volunteers. One possible reason for this may be that increased tortuosity, reported in the literature [10], may have been more prevalent in capillaries (diameter <10 μm) which were outside the detection range of our OCT system and thus were not monitored.

The studies that attempted to monitor blood velocity after radio/chemotherapy [8, 25, 40–45] mostly focused on early toxicity. Among those that investigated the late effects, all in animal models, there was little agreement on whether the flow increased or decreased after several months following irradiation [8, 42, 43, 45]. In the current study, we attempted to measure the average blood velocity in medium-sized vessels (i.e., arterioles and values) observable in Doppler OCT images. This quantitative analysis revealed a significant increase in average blood velocity in the medium-sized vessels in patients compared to the healthy volunteers. A possible explanation is that as the lumens of the medium-sized vessels decreased and total blood supply remained the same, the blood velocity had to increase to compensate for the decrease in lumen cross-section.

Patient imaging using OCT presented a number of technical challenges the most limiting of which were the ability to access the site of maximum tissue injury, patient's tolerance, and patient movement. The soft palate usually was in a volume of high dose radiation and was used as a surrogate of late tissue effects but in three patients, due to trismus or limited range of motion in the neck muscles (because of fibrosis), it could not be accessed. One way to address this obstacle is to use flexible probes of smaller diameters to facilitate access to various oral regions, such as the soft palate, without the need for a certain neck angle. Although the imaging procedure was easy, straightforward and non-hazardous, the total time required (20–45 min) was too long for some of patients. This prevented the acquisition of a sufficient number of datasets from these patients, rendering their data inadequate for analysis. Finally, keeping motionless was extremely difficult for some of the 15 patients in the study. This imposed an extra challenge for 3D dataset collection, especially when gathering svOCT maps of microvasculature as these required longer imaging times (~6 s for a volumetric dataset). This susceptibility to motion can, however, be reduced using novel OCT systems with higher A-scan and data acquisition rates.

While the developed system provided micron-scale resolution structural profiles and high-sensitivity vascular images, its lateral field-of-view was limited to $1\times1\ mm^2$. This made it impossible to image large tissue volumes and provide standard clinical images interpretable by the clinicians. However, by taking several smaller datasets from various heavily irradiated oral regions, calculating the quantitative metrics in all of them, and averaging these metrics over all, we provided an objective assessment method, based on quantitative analysis as opposed to subjective interpretation of images.

In calculating the four metrics, the procedures were partly computerized (using MATLAB or ImageJ) but still required (minimal) manual input from trained personnel,

typically involving layer or region delineation. The latter may have introduced a slight human bias and slowed down the quantification process. Therefore, one of the major steps for translating this technology and quantification platform to the clinic is to automate the entire metric calculation process. This can potentially lead to some level of error reduction, decrease the processing time, and make the system more adoptable and robust for clinical deployment.

In interpreting the obtained results, an issue arises as to whether the observed significant changes are restricted to regions with symptomatic late toxicity (which are often the regions that received >50 Gy), or if they occur as frequently in the low dose (mean dose ~35 Gy) regions as well. To address this issue, the three metrics that showed significant difference between patients and volunteers were calculated for a high dose (ipsilateral, ~52 Gy) and low dose (contralateral, <25 Gy) region in one of the patients (case #10) who was chosen randomly. The value for all three metrics (Ep/LP thickness, blood velocity, and vessel diameter) calculated on the contralateral side showed a smaller change than the ones on the ipsilateral side when compared to the healthy volunteers, as expected. Therefore, preliminary observation shows that as the radiation dose increases, the values calculated for each metric deviates more from normal. However, to draw a more robust conclusion on how OCT images and image-based metrics change as a function of radiation dose, a comparative study on a higher number of patients needs to be performed.

Since this tool promises to facilitate monitoring late radiation toxicity tissue changes well before debilitating symptoms occur on tissue surface, it may be possible to be used to assess tissue changes in other accessible organs such as the rectum or skin. Moreover, in patients with established radiation complications, this tool may be used as a complementary method to visual examination towards tracking tissue responses to medical interventions.

5 Conclusion

OCT imaging and image quantification techniques can highlight changes in the oral microstructural and microvascular features of late oral radiation toxicity patients compared to healthy volunteers. In this feasibility study, the significant differences observed in the oral tissue layer thickness and structure, as well as vessel morphology corresponded well with the expected histological changes discussed in the literature. Therefore, the OCT imaging platform and the assessment metrics show promise as a potential clinical noninvasive subsurface imaging tool that can be used as a complementary technique for early detection and diagnosis of late oral radiation toxicity, as well as monitoring the outcome of prescribed curative treatments for these patients.

Acknowledgments: The authors would like to thank the patients and volunteers who participated in this study as well as the funding sources: Natural Sciences and Engineering Research Council of Canada (NSERC)/ Canadian Institutes of Health Research (CIHR) through the Collaborative Health Research Program (CHRP) (Grant number: J365581-09) and Ministry of Education and Science of the Russian Federation (Grant number: 14.B25.31.0015).

Conflict of interest statement: The authors state no conflict of interest. All authors have read the journal's Publication Ethics and Publication Malpractice Statement available at the journal's website and hereby confirm that they comply with all its parts applicable to the present scientific work.

References

[1] Denis F, Garaud P, Bardet E, Alfonsi M, Sire C, Germain T, Bergerot P, Rhein B, Tortochaux J, Oudinot P, Calais G. Late toxicity results of the GORTEC 94-01 randomized trial comparing radiotherapy with concomitant radiochemotherapy for advanced-stage oropharynx carcinoma: comparison of LENT/ SOMA, RTOG/EORTC, and NCI-CTC scoring systems. Int J Radiat Oncol Biol Phys 2003;55(1):93–8.

[2] Meyer F, Fortin A, Wang CS, Liu G, Bairati I. Predictors of severe acute and late toxicities in patients with localized head-and-neck cancer treated with radiation therapy. Int J Radiat Oncol Biol Phys 2012;82(4):1454–62.

[3] Sciubba JJ, Goldenberg D. Oral complications of radiotherapy. Lancet Oncol 2006;7(2):175–83.

[4] Chao KS, Majhail N, Huang CJ, Simpson JR, Perez CA, Haughey B, Spector G. Intensity-modulated radiation therapy reduces late salivary toxicity without compromising tumor control in patients with oropharyngeal carcinoma: a comparison with conventional techniques. Radiother Oncol 2001;61(3):275–80.

[5] Specht L. Oral complications in the head and neck radiation patient. Introduction and scope of the problem. Support Care Cancer 2002;10(1):36–9.

[6] Stone HB, Coleman CN, Anscher MS, McBride WH. Effects of radiation on normal tissue: consequences and mechanisms. Lancet Oncol 2003;4(9):529–36.

[7] Mosel DD, Bauer RL, Lynch DP, Hwang ST. Oral complications in the treatment of cancer patients. Oral Dis 2011;17(6):550–9.

[8] Fajardo LF, Berthrong M, Anderson RE. Radiation pathology. New York: Oxford University Press, Inc.; 2001.
[9] Rodemann HP, Blaese MA. Responses of normal cells to ionizing radiation. Semin Radiat Oncol 2007;17(2):81–8.
[10] Baker DG, Krochak RJ. The response of the microvascular system to radiation: a review. Cancer Invest 1989;7(3):2 87–94.
[11] O'Sullivan B, Levin W. Late radiation-related fibrosis: pathogenesis, manifestations, and current management. Semin Radiat Oncol 2003;13(3):274–89.
[12] Fajardo LF. Basic mechanisms and general morphology of radiation injury. Semin Roentgenol 1993;28(4):297–302.
[13] Yang X, Tridandapani S, Beitler JJ, Yu DS, Yoshida EJ, Curran WJ, Liu T. Ultrasound GLCM texture analysis of radiation-induced parotid-gland injury in head-and-neck cancer radiotherapy: an in vivo study of late toxicity. Med Phys 2012;39(9):5732–9.
[14] Ying M, Wu VW, Kwong DL. Comparison of sonographic appearance of normal and postradiotherapy parotid glands: a preliminary study. Ultrasound Med Biol 2007;33(8):1244–50.
[15] Cheng SC, Wu VW, Kwong DL, Ying MT. Assessment of post-radiotherapy salivary glands. Br J Radiol 2011;84(1001): 393–402.
[16] Astreinidou E, Roesink JM, Raaijmakers CP, Bartels LW, Witkamp TD, Lagendijk JJ, Terhaard CH. 3D MR sialography as a tool to investigate radiation-induced xerostomia: feasibility study. Int J Radiat Oncol Biol Phys 2007;68(5):1310–9.
[17] Houweling AC, Schakel T, van den Berg CA, Philippens ME, Roesink JM, Terhaard CH, Raaijmakers CP. MRI to quantify early radiation-induced changes in the salivary glands. Radiother Oncol 2011;100(3):386–9.
[18] Bronstein AD, Nyberg DA, Schwartz AN, Shuman WP, Griffin BR. Increased salivary gland density on contrast-enhanced CT after head and neck radiation. AJR Am J Roentgenol 1987;149(6):1259–63.
[19] Juan CJ, Chen CY, Jen YM, Liu HS, Liu YJ, Hsueh CJ, Wang CY, Chou YC, Chai YT, Huang GS, Chung HW. Perfusion characteristics of late radiation injury of parotid glands: quantitative evaluation with dynamic contrast-enhanced MRI. Eur Radiol 2009;19(1):94–102.
[20] Drexler W, Fujimoto JG, editors. Optical coherence tomography: technology and applications. Berlin: Springer; 2008.
[21] Gladkova N, Maslennikova A, Balalaeva I, Feldchtein F, Kiseleva E, Karabut M, Iksanov R. Application of optical coherence tomography in the diagnosis of mucositis in patients with head and neck cancer during a course of radio(chemo)therapy. Med Laser Appl 2008;23(4):186–95.
[22] Lee CK, Tsai MT, Lee HC, Chen HM, Chiang CP, Wang YM, Yang CC. Diagnosis of oral submucous fibrosis with optical coherence tomography. J Biomed Opt 2009;14(5):054008.
[23] Muanza TM, Cotrim AP, McAuliffe M, Sowers AL, Baum BJ, Cook JA, Feldchtein F, Amazeen P, Coleman CN, Mitchell JB. Evaluation of radiation-induced oral mucositis by optical coherence tomography. Clin Cancer Res 2005;11(14):5121–7.
[24] Tsai MT, Lee CK, Lee HC, Chen HM, Chiang CP, Wang YM, Yang CC. Differentiating oral lesions in different carcinogenesis stages with optical coherence tomography. J Biomed Opt 2009;14(4):044028.
[25] Wilder-Smith P, Hammer-Wilson MJ, Zhang J, Wang Q, Osann K, Chen Z, Wigdor H, Schwartz J, Epstein J. In vivo imaging of oral mucositis in an animal model using optical coherence tomography and optical Doppler tomography. Clin Cancer Res 2007;13(8):2449–54.
[26] Calantog A, Hallajian L, Nabelsi T, Mansour S, Le A, Epstein J, Wilder-Smith P. A prospective study to assess in vivo optical coherence tomography imaging for early detection of chemotherapy-induced oral mucositis. Lasers Surg Med 2013;45(1):22–7.
[27] Clinical trial number NCT01692600. Optical coherence tomography for monitoring late oral radiation toxicity after radiotherapy of head and neck cancer patients. https://www.clinicaltrials.gov/ct2/show/NCT01692600?term=cross-sectional+feasibility+study+OCT&rank=1 [Accessed on September 24, 2015].
[28] Davoudi B, Lindenmaier A, Standish BA, Allo G, Bizheva K, Vitkin A. Noninvasive in vivo structural and vascular imaging of human oral tissues with spectral domain optical coherence tomography. Biomed Opt Express 2012;3(5): 826–39.
[29] Laser Institute of America. American National Standard for Safe Use of Lasers. ANSI® Z136.1 – 2007. https://www.lia.org/PDF/Z136_1_s.pdf [Accessed on July 29, 2015].
[30] Ridgway JM, Armstrong WB, Guo S, Mahmood U, Su J, Jackson RP, Shibuya T, Crumley RL, Gu M, Chen Z, Wong BJ. In vivo optical coherence tomography of the human oral cavity and oropharynx. Arch Otolaryngol Head Neck Surg 2006;132(10):1074–81.
[31] Zhao Y, Chen Z, Saxer C, Xiang S, de Boer JF, Nelson JS. Phase-resolved optical coherence tomography and optical Doppler tomography for imaging blood flow in human skin with fast scanning speed and high velocity sensitivity. Opt Lett 2000;25(2):114–6.
[32] Yang V, Gordon M, Qi B, Pekar J, Lo S, Seng-Yue E, Mok A, Wilson B, Vitkin I. High speed, wide velocity dynamic range Doppler optical coherence tomography (Part I): System design, signal processing, and performance. Opt Express 2003;11(7):794–809.
[33] Mahmud MS, Cadotte DW, Vuong B, Sun C, Luk TW, Mariampillai A, Yang VX. Review of speckle and phase variance optical coherence tomography to visualize microvascular networks. J Biomed Opt 2013;18(5):50901.
[34] Davoudi B, Morrison M, Bizheva K, Yang VX, Dinniwell R, Levin W, Vitkin IA. Optical coherence tomography platform for microvascular imaging and quantification: initial experience in late oral radiation toxicity patients. J Biomed Opt 2013;18(7):76008.
[35] Xu J, Wong K, Jian Y, Sarunic MV. Real-time acquisition and display of flow contrast using speckle variance optical coherence tomography in a graphics processing unit. J Biomed Opt 2014;19(2):026001.
[36] Mariampillai A, Leung MK, Jarvi M, Standish BA, Lee K, Wilson BC, Vitkin A, Yang VX. Optimized speckle variance OCT imaging of microvasculature. Opt Lett 2010;35(8):1257–9.
[37] Davoudi B, Damodaran V, Bizheva K, Yang V, Dinniwell R, Levin W, Vitkin A. Development of quantitative parameters to assess in-vivo optical coherence tomography images of late oral radiation toxicity patients. Proc SPIE 2013;8565:856525. doi: 10.1117/12.2001124.
[38] Glantz SA. Primer of biostatistics. San Francisco: McGraw-Hill; 1997.

[39] Davoudi B, Bizheva K, Wong A, Dinniwell R, Levin W, Vitkin IA. Correlating optical coherence tomography images with dose distribution in late oral radiation toxicity patients. Photonics Lasers Med 2014;3(4):311–21.
[40] Reinhold HS. The influence of radiation on blood vessels and circulation. Chapter IV. Structural changes in blood vessels. Curr Top Radiat Res Q 1974;10(1):58–74.
[41] Acker JC, Marks LB, Spencer DP, Yang W, Avery MA, Dodge RK, Rosner GL, Dewhirst MW. Serial in vivo observations of cerebral vasculature after treatment with a large single fraction of radiation. Radiat Res 1998;149(4):350–9.
[42] Dimitrievich GS, Fischer-Dzoga K, Griem ML. Radiosensitivity of vascular tissue. I. Differential radiosensitivity of capillaries: a quantitative in vivo study. Radiat Res 1984;99(3):511–35.
[43] Nguyen V, Gaber MW, Sontag MR, Kiani MF. Late effects of ionizing radiation on the microvascular networks in normal tissue. Radiat Res 2000;154(5):531–6.
[44] Hamilton S, Yoo J, Hammond A, Read N, Venkatesan V, Franklin J, Fung K, Gray D, Parry N, Van Diepen K, Baswick BL, Badhwar A. Microvascular changes in radiation-induced oral mucositis. J Otolaryngol Head Neck Surg 2008;37(5):730–7.
[45] Law MP. Radiation-induced vascular injury and its relation to late effects in normal tissues. Adv Radiat Biol 1981;9:37–73.

Supplemental Material: The online version of this article (DOI: 10.1515/plm-2015-0025) offers supplementary material, available to authorized users.